

Scaling of the Quantum Geometry Metrics in Disordered Topological Phases

Jorge Martínez Romeral,^{1,2} Aron W. Cummings,¹ and Stephan Roche^{1,3}

¹*Catalan Institute of Nanoscience and Nanotechnology (ICN2),
CSIC and BIST, Campus UAB, Bellaterra, 08193 Barcelona, Spain*

²*Department of Physics, Campus UAB, Bellaterra, 08193 Barcelona, Spain*

³*ICREA–Institució Catalana de Recerca i Estudis Avançats, 08010 Barcelona, Spain*

(Dated: June 19, 2024)

We report a study of disorder-dependent quantum geometry in topological systems. Thanks to the development of an efficient linear-scaling numerical methodology based on the kernel polynomial method, we can explore the nontrivial behavior of the quantum geometry metrics (quantum metric and Chern number) in large-scale inhomogeneous systems, accounting for the presence of disorder. We illustrate this approach in the disordered Haldane model, examining the impact of Anderson and vacancy-type of disorders on the trivial and topological phases captured by this model.

Introduction. During the last decades, the Berry curvature has been the cornerstone of topological matter [1, 2]. But recently, it has been shown that it is only one of two parts, the imaginary part, of a more general structure called the quantum geometric tensor (QGT). The real part of the QGT, usually called the quantum metric, has received a lot of attention lately as it has been shown to play a crucial role in the superconductivity of flat band materials [3–7], electron-phonon coupling [8], linear [9–12] and nonlinear response theory [13–16], and a large compendium of other effects [17]. The quantum metric is a key quantity in the modern theory of insulators, as it is directly related to the real-space localization of the ground state [18–21]. Moreover, the quantum metric has been proven to be especially useful for bounding quantities since it is bounded from below by the Chern number [3, 22, 23]. In addition, the QGT has been already experimentally investigated and its connection to various observables has been demonstrated [14, 24–28].

Although the Berry curvature has been widely studied in the presence of disorder [29–31], the properties and scaling of the quantum metric as a function of disorder are mostly unexplored to date. As disorder is known to induce localization effects in low-dimensional systems [32, 33], and since the quantum metric is a direct measure of the localization of the ground state [18], the behavior of the disorder-dependent quantum metric is expected to provide relevant information for understanding transport properties. However, such studies are scarce [21, 34], and little is known for disordered topological phases.

In this Letter, we develop a computationally efficient approach to calculating the quantum geometric tensor of large, arbitrarily-disordered systems. We then apply this method to the study of the Haldane Hamiltonian [35, 36] in the presence of various sources of disorder. By tuning the Hamiltonian’s parameters, we study the impact of disorder on both the nontrivial Chern insulating phase and the topologically trivial phase. Disorder is introduced either via the random Anderson potential [32], or through a random distribution of vacancies.

To account for the disorder-induced breaking of trans-

lational invariance and to simulate large system sizes, we employ a real-space linear-scaling method based on the kernel polynomial method (KPM) [37]. This method is similar to implementations of the real-space Chern marker [30, 38] based on the expansion of the ground state projector [30]. However, in contrast with previous methods [30, 38, 39], our approach allows *both open and periodic boundary conditions*. Our method also gives access to the spatially-resolved QGT, hence informing about its real space behavior and fluctuations.

Our findings reveal that the QGT, and in particular the quantum metric, can display nontrivial behavior in the presence of disorder, enabling localization or delocalization depending on the disorder strength and the topological phase. This is also displayed in the real-space projection of the quantum metric, which offers more precise understanding of the quantity. Looking ahead, this method may be used to explore other types of materials, such as Moiré systems in which disorder effects could be key in understanding their emergent properties.

Components of the quantum geometric tensor. In periodic systems, the QGT can be written as a momentum-dependent quantity, $Q_{\alpha\beta}(\mathbf{k}) = \sum_{ij} f_{i\mathbf{k}}(1 - f_{j\mathbf{k}}) \langle \psi_{i\mathbf{k}} | \partial_{k_\alpha} \hat{H} | \psi_{j\mathbf{k}} \rangle \langle \psi_{j\mathbf{k}} | \partial_{k_\beta} \hat{H} | \psi_{i\mathbf{k}} \rangle / (E_{i\mathbf{k}} - E_{j\mathbf{k}})^2$, where \hat{H} is the Hamiltonian, $|\psi_{i\mathbf{k}}\rangle$ is the eigenstate of \hat{H} in band i at momentum \mathbf{k} , $E_{i\mathbf{k}}$ its corresponding eigenenergy, and $f_{i\mathbf{k}}$ is its occupation factor. The QGT can be separated into two parts [40],

$$Q_{\alpha\beta}(\mathbf{k}) = g_{\alpha\beta}(\mathbf{k}) + \frac{i}{2} \Omega_{\alpha\beta}(\mathbf{k}), \quad (1)$$

where $\Omega_{\alpha\beta}(\mathbf{k})$ is the antisymmetric imaginary part, usually called the Berry curvature, and $g_{\alpha\beta}(\mathbf{k})$ is the real symmetric part, known as the quantum metric [40].

Because the QGT is a positive semi-definite matrix [41], both the Berry curvature and the quantum metric are related via the inequality $\text{Tr} g_{\alpha\beta}(\mathbf{k})/2 \geq |\Omega_{\alpha\beta}(\mathbf{k})|$ [3]. This can be integrated over the first Brillouin zone, giving $\text{Tr} \mathcal{G}_{\alpha\beta} \geq \mathcal{C}$, where $\mathcal{G}_{\alpha\beta} = \int_{\text{BZ}} d\mathbf{k} g_{\alpha\beta}(\mathbf{k})/4\pi$ is known as the integrated quantum metric (IQM) and $\mathcal{C} = \int_{\text{BZ}} d\mathbf{k} \Omega_{\alpha\beta}(\mathbf{k})/2\pi$ is the Chern number [42, 43].

The integrated quantum metric can be related to the invariant part of the spread of the maximally localized Wannier functions [20], which in two dimensions (2D) can be expressed as $\Omega_I = A/\pi \cdot \text{Tr} \mathcal{G}_{\alpha\beta}$, where A is the area of the system. The IQM is the keystone of the modern theory of insulators [18, 19], which states that the dimensionless quantity $\text{Tr} \mathcal{G}_{\alpha\beta}$ diverges in the thermodynamic limit ($A \rightarrow \infty$) for metals and converges to a finite value for any kind of insulator.

The QGT can also be expressed as the fluctuation of the position operator in the ground state [44],

$$\mathcal{Q}_{\alpha\beta} = \frac{1}{A} (\langle \hat{r}_\alpha \hat{r}_\beta \rangle - \langle \hat{r}_\alpha \rangle \langle \hat{r}_\beta \rangle), \quad (2)$$

where \hat{r}_α is the position operator in the α direction. In periodic systems, this expression for $\mathcal{Q}_{\alpha\beta}$ is equal to that of Eq. (1) integrated over the Brillouin zone. However, Eq. (2) is also applicable to systems without translational invariance, allowing the study of disorder effects.

The relation of the IQM with the Wannier spread, and the fluctuation of the position operator, indicates that the IQM is a measure of the localization properties of the ground state. A low IQM implies localized Wannier functions, while a higher IQM suggests more delocalized electronic states and more extended position fluctuations, which in the thermodynamic limit may be an indicator of metallic behavior. This suggests that changes to the IQM in the presence of disorder may be an indicator of the transport properties of the system.

Linear-scaling calculation of the QGT. In periodic systems, computing the QGT via Eq. (1) relies on diagonalization of the Bloch Hamiltonian, which can become computationally expensive for systems with large unit cells. In addition, in systems with open boundary conditions or with disorder, where periodicity is broken, direct calculation of Eq. (2) relies on brute-force diagonalization of huge real-space Hamiltonians, which significantly restricts the accessible system sizes.

Here we efficiently calculate the QGT in large-area disordered systems by considering its real-space form [19],

$$\mathcal{Q}_{\alpha\beta} = -\frac{1}{A} \text{Tr} \left\{ \hat{P} \left[\hat{r}_\alpha, \hat{P} \right] \left[\hat{r}_\beta, \hat{P} \right] \right\}, \quad (3)$$

where $\hat{P} = \hat{\Theta}(\hat{H} - E_F)$ is the zero-temperature ground state projector and E_F is the Fermi energy of the system. To avoid direct diagonalization, we expand this operator as a series of Chebyshev polynomials [37], $\hat{A}(\hat{H}) \approx \sum_{m=0}^M g_m \mu_m \hat{T}_m(\hat{H})$, where \hat{H} has been normalized such that its spectrum lies in $[-1, 1]$, T_m is the m th-order Chebyshev polynomial, g_m are the coefficients of the Jackson kernel, used to damp Gibbs oscillations [45], and the moments μ_m have an exact analytical form [30].

Previous implementations of similar formulas, to calculate the so-called topological markers [30, 38, 39], relied on open boundary conditions since the position operator

is ill-defined for periodic boundary conditions. Here, by using the recurrence relation of the Chebyshev polynomials, the commutator $[\hat{r}_\alpha, \hat{P}]$ can be expressed in terms of the velocity operator $\hat{v}_\alpha = [\hat{r}_\alpha, \hat{H}]/i\hbar$, which is well defined independent of the boundary conditions [46]. In our calculations below, we are thus free to use periodic boundary conditions and avoid edge effects while reaching systems containing millions of atoms.

Finally, we use the stochastic trace approximation [37, 45] to efficiently evaluate the trace of Eq. (3). The integrated quantum metric is then given by $\mathcal{G}_{\alpha\beta} = 4\pi \text{Re}\{\mathcal{Q}_{\alpha\beta}\}$, and the Chern number by $\mathcal{C} = 4\pi \epsilon^{\alpha\beta} \text{Im}\{\mathcal{Q}_{\beta\alpha}\}$, where $\epsilon^{\alpha\beta}$ is the Levi-Civita symbol. In practice, the Chebyshev polynomial expansion is only performed for a finite number of moments M . In the following, we have made sure that all of our calculations are converged with respect to both system size and number of moments, as shown in the SM [46]. Equation (3) is the trace over an operator in the real-space basis, and thus each element in the trace allows us to also construct a real-space map of the quantum metric, similar to what has been done for the local Chern marker [30, 38, 39].

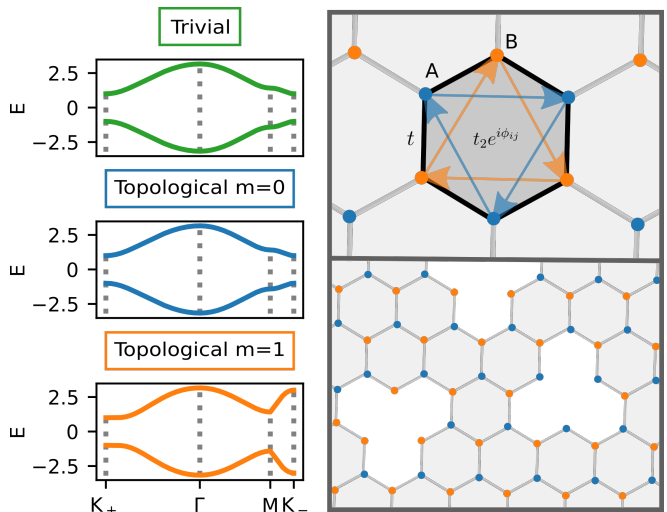


FIG. 1. Left panels: band structure of different phases of the Haldane model. Top panel: trivial phase with $\Delta_m = 1$ and $\Delta_H = 0$. Middle panel: topological phase with inversion symmetry, $\Delta_m = 0$ and $\Delta_H = 2$. Bottom panel: topological phase with broken inversion symmetry $\Delta_m = 2$ and $\Delta_H = 4$. Right panel: spatial representation (top) of the Haldane model where the arrows indicate the second nearest neighbor complex hoppings (blue/orange dots indicate the A/B sublattices); real space representation (bottom) of the Haldane model with vacancies.

Application to the disordered Haldane model. We now study the QGT in the disordered Haldane model, which is a tight-binding model in a honeycomb lattice with one orbital per atom [35], shown schematically in Fig. 1 (top

right panel). This model contains three terms,

$$\hat{H} = t \sum_{\langle ij \rangle} c_i^\dagger c_j \pm m \sum_{i \in A/B} c_i^\dagger c_i + t_2 \sum_{\langle\langle ij \rangle\rangle} e^{i\phi_{ij}} c_i^\dagger c_j + \text{h.c.} \quad (4)$$

The first term is a nearest-neighbor hopping term, where we arbitrarily set $t = 1$. All other energy scales in this work are thus relative to t . The second term, positive on sublattice A and negative on sublattice B (blue/orange dots in Fig. 1), breaks inversion symmetry and opens a trivial band gap $\Delta_m = 2m$. The third term is a complex second-neighbor hopping that breaks time-reversal symmetry and opens a topological gap $\Delta_H = 6\sqrt{3}t_2$ (here we set $\phi_{ij} = \pi/2$). When both gap-opening terms are nonzero, the total band gap is given by $\Delta = |\Delta_m - \Delta_H|$. When $\Delta_m > \Delta_H$ the system is a trivial insulator, otherwise it is a Chern insulator with $\mathcal{C} = 1$ [35, 42]. This model well describes the class of Chern insulators and the related quantum anomalous Hall phase [47, 48].

We now consider the three primary phases that emerge in this model. In the trivial phase, which is nothing more than gapped graphene, we let $\Delta_m = 2$ and $\Delta_H = 0$. In the topological phase with inversion symmetry, $\Delta_m = 0$ and $\Delta_H = 2$. Finally, in the topological phase with broken inversion symmetry, $\Delta_m = 2$ and $\Delta_H = 4$. This last phase has been shown to behave differently under the presence of disorder than the one without symmetry breaking [29]. The band structures of these three phases are shown in the left panels of Fig. 1. In all cases the total band gap is $\Delta = 2$.

Figure 2 (left panel) shows the Chern number, \mathcal{C} (dashed lines), and the trace of the IQM, $\text{Tr } \mathcal{G}$ (solid line), for the three phases of the Haldane model without disorder. As expected, $\mathcal{C} = 1$ in the topological phases for energies inside the gap, and is zero for the trivial phase. Meanwhile, broken inversion symmetry extends the topological phase ($\mathcal{C} > 0$) to a higher range of energies. In this phase, the K_\pm valleys have different gaps, $\Delta = 2$ and 6 respectively (bottom left panel of Fig. 1). For energies in the range $E_F \in [-3, 3]$, only the K_+ valley contributes and thus the Chern number is finite for a wider range of energies than for the $m = 0$ topological phase.

On the other hand, the IQM is nonzero both inside and outside the gap, and is bounded from below by the Chern number in all cases. Within the gap, the IQM is reduced in the trivial phase compared to the topological phases, indicating a higher degree of electronic localization. Outside the gap, the system is metallic and the wave functions are delocalized, as our numerical scaling analysis reveals a divergent quantum metric in the thermodynamic limit [18, 46].

We next consider the impact of Anderson disorder on the QGT [32], which is treated as a random onsite potential, $\hat{H}_W = \sum_i \epsilon_i c_i^\dagger c_i$, where ϵ_i are randomly distributed in the interval $\epsilon_i \in [-W/2, W/2]$. In two dimensions, such disorder leads to a metal-insulator tran-

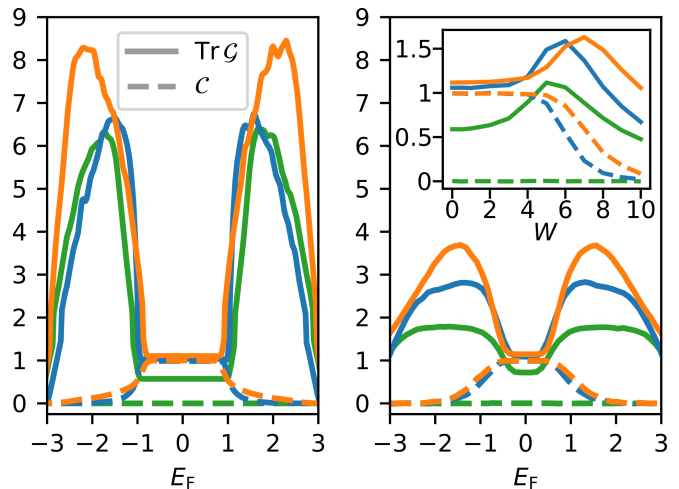


FIG. 2. Left panel: IQM (solid lines) and Chern number (dashed lines) vs. Fermi energy without disorder. The trivial, purely topological ($m = 0$), and inversion-symmetry-broken topological ($m = 1$) phases are shown in green, blue, and orange. Right panel: IQM and Chern number vs. Fermi energy with an Anderson disorder of $W = 3$. Inset: IQM and Chern number as a function of disorder strength at $E_F = 0$.

sition for which all states are localized whatever their energy [49]. Figure 2 (right panel) shows the IQM and the Chern number for Anderson disorder strength $W = 3$. Here we see that the gap is shrunk, owing to disorder-induced broadening and the introduction of in-gap localized states. Outside the gap, the IQM is strongly suppressed in all cases. A scaling analysis shows that these states that were metallic in the disorder-free case have now become localized in the limit $M, A \rightarrow \infty$ [46], as expected for the Anderson metal-insulator transition.

The inset of Fig. 2 shows \mathcal{C} and the IQM for varying disorder strength at the middle of the gap ($E_F = 0$). Both quantities are robust for a wide range of disorder and only decay for disorder strength larger than the energy gap ($W \gtrsim 4$). The topological phase with broken inversion symmetry exhibits the slowest decay with disorder, as well as the highest overall values. These two behaviors may be linked to the absence of intervalley scattering in this phase; as states experience fewer scattering events, localization effects are reduced.

We also see that for $W \lesssim 4$, the IQM actually increases with increasing disorder for all phases. This may be attributed to the mixing of states into the gap, via the disorder-induced broadening. For low values of W , the localization length of these states is expected to be longer than the in-gap states, effectively increasing the IQM. At higher values of W , Anderson localization then fully takes over. A similar effect has also been observed in disordered twisted bilayer graphene at magic angle [21].

Finally, we explore the impact of vacancy defects, shown schematically in Fig. 1 (bottom right panel). Vacancies are modeled by randomly removing $n \cdot N$ lattice

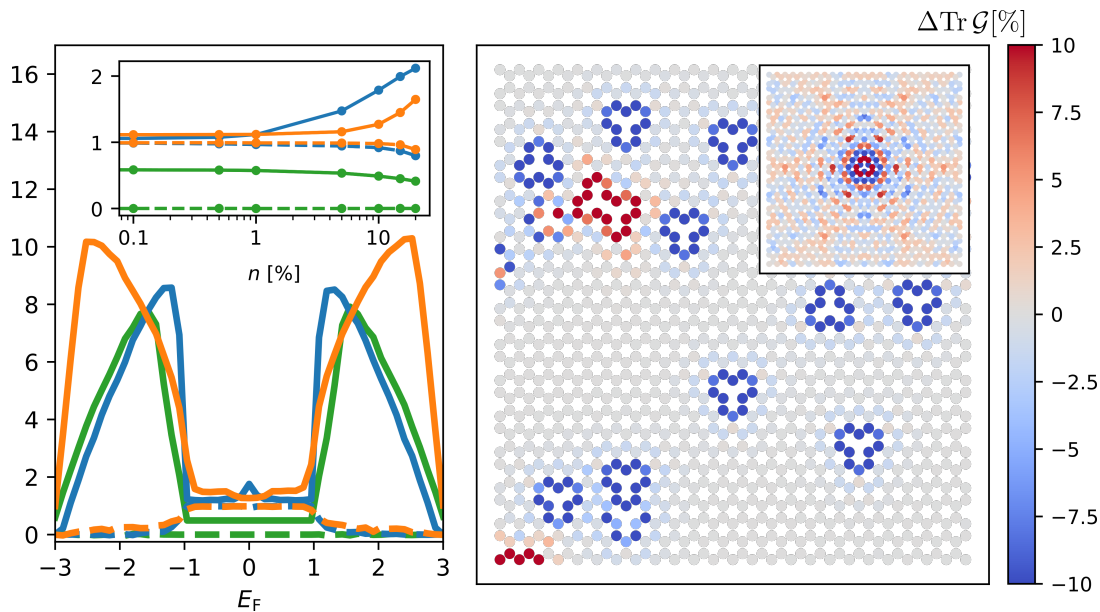


FIG. 3. Left panel: IQM (solid lines) and Chern number (dashed lines) vs. Fermi energy for a vacancy concentration of $n = 10\%$. The trivial, purely topological ($m = 0$), and inversion-symmetry-broken topological ($m = 1$) phases are shown in green, blue, and orange. Left inset: IQM and Chern number for $n \in [0.1, 20\%]$ at $E_F = 0$. Right panel: real-space fluctuations of the IQM, $\Delta \text{Tr} \mathcal{G} = 100\% \cdot (\text{Tr} \mathcal{G} - \text{Tr} \mathcal{G}_{\text{clean}}) / \text{Tr} \mathcal{G}_{\text{clean}}$, for $n = 1\%$ of vacancies in the topological phase with $m = 0$ at $E_F = 0$. Inset: real-space fluctuations of the IQM around a single impurity at high energy, $E_F = 2$.

sites, where n is the vacancy concentration and N is the number of atoms in the clean system. Their impact on quantum transport has been well scrutinized in Dirac materials, with the presence of zero energy modes leading to nontrivial transport phenomena [34, 50, 51].

Figure 3 (left panel) shows the IQM and the Chern number for a vacancy concentration of $n = 10\%$, and the inset shows the same quantities at $E_F = 0$ for $n \in [0.1, 20\%]$. For energies outside the gap, the IQM decreases dramatically in the presence of vacancies, similar to what was seen for Anderson disorder in Fig. 2. In the gap (see inset), different behaviors develop depending on the phase of the system. In the trivial phase, the IQM is weakly reduced with increasing vacancy concentration, while in the topological phases the IQM first slightly decreases and then eventually increases for larger vacancy concentration, with this increase sharper in the phase without broken inversion symmetry ($m = 0$).

To understand this behavior, we scrutinize the real-space distribution of the IQM (right panel of Fig. 3) for the purely topological phase ($m = 0$) at $E_F = 0$ for a vacancy concentration of $n = 1\%$ (corresponding densities of states (DOS) are shown in the SM [46]). In this phase, vacancies locally reduce the IQM and introduce in-gap impurity states which originate from the bulk-edge correspondence [52, 53]. At high vacancy concentration, the real space projection enables us to understand the increase in the IQM, as neighboring impurity states are more likely to overlap (dark red region in the right panel), yielding an enhancement of delocalization consist-

ent with the increase of the IQM seen in the left panel. The real space projection when a high number of vacancies is present ($n = 10\%$) is shown in the SM [46].

In the topological phase with broken inversion symmetry ($m = 1$), vacancies create two peaks in the DOS at $E_F = \pm 0.31$ [46], as the A and B sites are no longer equivalent. Similar to the Anderson disorder case, this phase is generally less localized than the pure topological phase. This weak dependence on disorder is also seen at the energies where the impurities peaks appear [46]. As these impurity peaks are localized on the A or B sublattice, such behavior may be connected to prior studies in graphene and topological insulators indicating that vacancies or hydrogen defects distributed on only one sublattice have a weaker impact than those evenly distributed on both [34, 53–56]. Finally, the IQM in the trivial phase is only weakly reduced, as there is no formation of in-gap states because of the lack of edge states [53]. This leads to a weak scattering cross section and a relatively small impact on the IQM with increasing vacancy concentration [46].

The real-space projection at high energies (Fig. 3, right inset) reveals a long-range oscillatory behavior characteristic of Friedel oscillations [57–59]. This behavior is also present in the topological and trivial $m = 1$ phases [46], but further study is required to correlate such behavior with the resulting impact on transport.

Summary and outlook. We have introduced a numerically efficient linear-scaling algorithm based on the kernel polynomial method to compute the quantum ge-

ometric tensor in large and inhomogeneous systems. We have illustrated the method by exploring the scaling of the quantum geometry metrics in trivial and topological systems with Anderson disorder and vacancies. The quantum metric was verified to be lower bounded by the Chern number, while its scaling behavior with disorder provides information about localization-delocalization transitions, which depend on the nature and strength of disorder potential, as well as the topological phase. Our findings reveal that a topological phase with broken inversion symmetry exhibits higher resilience to disorder (due to the suppression of intervalley scattering), retaining its topological characteristics over a broader range of disorder strengths. Future work could extend these methods to explore other types of materials, such as topological semimetals, topological insulators or Moiré systems in which disorder effects could be key in understanding some of their emergent properties.

J.M.R. acknowledges P.A. Guerrero and L.M. Canonico for fruitful discussions. We acknowledge funding from MCIN/AEI /10.13039/501100011033 and European Union "NextGenerationEU/PRTR" under grant PCI2021-122035-2A-2a. ICN2 is funded by the CERCA Programme/Generalitat de Catalunya and supported by the Severo Ochoa Centres of Excellence programme, Grant CEX2021-001214-S, funded by MCIN/AEI/10.13039.501100011033. This work is also supported by MICIN with European funds-NextGenerationEU (PRTR-C17.I1) and by and 2021 SGR 00997, funded by Generalitat de Catalunya.

-
- [1] M. Kohmoto, Topological invariant and the quantization of the hall conductance, *Ann. Phys.* **160**, 343 (1985).
- [2] D. Xiao, M.-C. Chang, and Q. Niu, Berry phase effects on electronic properties, *Rev. Mod. Phys.* **82**, 1959 (2010).
- [3] S. Peotta and P. Törmä, Superfluidity in topologically nontrivial flat bands, *Nat. Commun.* **6**, 1 (2015).
- [4] A. Julku, T. J. Peltonen, L. Liang, T. T. Heikkilä, and P. Törmä, Superfluid weight and Berezinskii-Kosterlitz-Thouless transition temperature of twisted bilayer graphene, *Phys. Rev. B* **101**, 060505 (2020).
- [5] F. Xie, Z. Song, B. Lian, and B. A. Bernevig, Topology-Bounded Superfluid Weight in Twisted Bilayer Graphene, *Phys. Rev. Lett.* **124**, 167002 (2020).
- [6] P. Törmä, S. Peotta, and B. A. Bernevig, Superconductivity, superfluidity and quantum geometry in twisted multilayer systems, *Nat. Rev. Phys.* **4**, 528 (2022).
- [7] M. Long, A. Jimeno-Pozo, H. Sainz-Cruz, P. A. Pantaleon, and F. Guinea, Evolution of Superconductivity in Twisted Graphene Multilayers, [arXiv:2403.00903](https://arxiv.org/abs/2403.00903).
- [8] J. Yu, C. J. Ciccarino, R. Bianco, I. Errea, P. Narang, and B. A. Bernevig, Non-trivial quantum geometry and the strength of electron-phonon coupling, *Nat. Phys.* [10.1038/s41567-024-02486-0](https://doi.org/10.1038/s41567-024-02486-0) (2024).
- [9] I. Komissarov, T. Holder, and R. Queiroz, The quantum geometric origin of capacitance in insulators, *Nat. Commun.* **15**, 1 (2024).
- [10] N. Verma and R. Queiroz, Instantaneous Response and Quantum Geometry of Insulators, [arXiv:2403.07052](https://arxiv.org/abs/2403.07052).
- [11] F. Piéchon, A. Raoux, J.-N. Fuchs, and G. Montambaux, Geometric orbital susceptibility: Quantum metric without Berry curvature, *Phys. Rev. B* **94**, 134423 (2016).
- [12] A. Kruchkov, Quantum transport anomalies in dispersionless quantum states, *Phys. Rev. B* **107**, L241102 (2023).
- [13] D. Kaplan, T. Holder, and B. Yan, Unification of Nonlinear Anomalous Hall Effect and Nonreciprocal Magnetoresistance in Metals by the Quantum Geometry, *Phys. Rev. Lett.* **132**, 026301 (2024).
- [14] A. Gao, Y.-F. Liu, J.-X. Qiu, B. Ghosh, T. V. Trevisan, Y. Onishi, C. Hu, T. Qian, H.-J. Tien, S.-W. Chen, M. Huang, D. Bérubé, H. Li, C. Tzschaschel, T. Dinh, Z. Sun, S.-C. Ho, S.-W. Lien, B. Singh, K. Watanabe, T. Taniguchi, D. C. Bell, H. Lin, T.-R. Chang, C. R. Du, A. Bansil, L. Fu, N. Ni, P. P. Orth, Q. Ma, and S.-Y. Xu, Quantum metric nonlinear Hall effect in a topological antiferromagnetic heterostructure, *Science* **381**, 181 (2023).
- [15] N. Wang, D. Kaplan, Z. Zhang, T. Holder, N. Cao, A. Wang, X. Zhou, F. Zhou, Z. Jiang, C. Zhang, S. Ru, H. Cai, K. Watanabe, T. Taniguchi, B. Yan, and W. Gao, Quantum-metric-induced nonlinear transport in a topological antiferromagnet, *Nature* **621**, 487 (2023).
- [16] K. Das, S. Lahiri, R. B. Atencia, D. Culcer, and A. Agarwal, Intrinsic nonlinear conductivities induced by the quantum metric, *Phys. Rev. B* **108**, L201405 (2023).
- [17] P. Törmä, Essay: Where Can Quantum Geometry Lead Us?, *Phys. Rev. Lett.* **131**, 240001 (2023).
- [18] R. Resta, The insulating state of matter: a geometrical theory, *Eur. Phys. J. B* **79**, 121 (2011).
- [19] A. Marrazzo and R. Resta, Local Theory of the Insulating State, *Phys. Rev. Lett.* **122**, 166602 (2019).
- [20] N. Marzari and D. Vanderbilt, Maximally localized generalized Wannier functions for composite energy bands, *Phys. Rev. B* **56**, 12847 (1997).
- [21] P. A. Guerrero, V.-H. Nguyen, J. M. Romeral, A. W. Cummings, J.-H. Garcia, J.-C. Charlier, and S. Roche, Disorder-Induced Delocalization in Magic-Angle Twisted Bilayer Graphene, [arXiv:2401.08265](https://arxiv.org/abs/2401.08265).
- [22] R. Roy, Band geometry of fractional topological insulators, *Phys. Rev. B* **90**, 165139 (2014).
- [23] Y. Onishi and L. Fu, Fundamental Bound on Topological Gap, *Phys. Rev. X* **14**, 011052 (2024).
- [24] X. Tan, D.-W. Zhang, Z. Yang, J. Chu, Y.-Q. Zhu, D. Li, X. Yang, S. Song, Z. Han, Z. Li, Y. Dong, H.-F. Yu, H. Yan, S.-L. Zhu, and Y. Yu, Experimental Measurement of the Quantum Metric Tensor and Related Topological Phase Transition with a Superconducting Qubit, *Phys. Rev. Lett.* **122**, 210401 (2019).
- [25] M. Kolodrubetz, V. Gritsev, and A. Polkovnikov, Classifying and measuring geometry of a quantum ground state manifold, *Phys. Rev. B* **88**, 064304 (2013).
- [26] M. Yu, P. Yang, M. Gong, Q. Cao, Q. Lu, H. Liu, S. Zhang, M. B. Plenio, F. Jelezko, T. Ozawa, N. Goldman, and J. Cai, Experimental measurement of the quantum geometric tensor using coupled qubits in diamond, *Natl. Sci. Rev.* **7**, 254 (2020).
- [27] C.-R. Yi, J. Yu, H. Yuan, R.-H. Jiao, Y.-M. Yang, X. Jiang, J.-Y. Zhang, S. Chen, and J.-W. Pan, Extracting the quantum geometric tensor of an optical Raman

- lattice by Bloch-state tomography, *Phys. Rev. Res.* **5**, L032016 (2023).
- [28] A. Gianfrate, O. Bleu, L. Dominici, V. Ardizzone, M. De Giorgi, D. Ballarini, G. Lerario, K. W. West, L. N. Pfeiffer, D. D. Solnyshkov, D. Sanvitto, and G. Malpuech, Measurement of the quantum geometric tensor and of the anomalous Hall drift, *Nature* **578**, 381 (2020).
- [29] J. H. García, L. Covaci, and T. G. Rappoport, Real-Space Calculation of the Conductivity Tensor for Disordered Topological Matter, *Phys. Rev. Lett.* **114**, 116602 (2015).
- [30] D. Varjas, M. Fruchart, A. R. Akhmerov, and P. M. Perez-Piskunow, Computation of topological phase diagram of disordered $\text{Pb}_{1-x}\text{Sn}_x\text{Te}$ using the kernel polynomial method, *Phys. Rev. Res.* **2**, 013229 (2020).
- [31] E. V. Castro, M. P. López-Sancho, and M. A. H. Vozmediano, Anderson localization and topological transition in Chern insulators, *Phys. Rev. B* **92**, 085410 (2015).
- [32] P. W. Anderson, Absence of Diffusion in Certain Random Lattices, *Phys. Rev.* **109**, 1492 (1958).
- [33] A. Lagendijk, B. v. Tiggelen, and D. S. Wiersma, Fifty years of Anderson localization, *Phys. Today* **62**, 24 (2009).
- [34] Q. Marsal and A. M. Black-Schaffer, Enhanced quantum metric due to vacancies in graphene, [arXiv:2406.01408](https://arxiv.org/abs/2406.01408).
- [35] F. D. M. Haldane, Model for a Quantum Hall Effect without Landau Levels: Condensed-Matter Realization of the "Parity Anomaly", *Phys. Rev. Lett.* **61**, 2015 (1988).
- [36] D. N. Sheng, Z. Y. Weng, L. Sheng, and F. D. M. Haldane, Quantum spin-hall effect and topologically invariant chern numbers, *Phys. Rev. Lett.* **97**, 036808 (2006).
- [37] Z. Fan, J. H. Garcia, A. W. Cummings, J. E. Barrios-Vargas, M. Panhans, A. Harju, F. Ortmann, and S. Roche, Linear scaling quantum transport methodologies, *Phys. Rep.* **903**, 1 (2021).
- [38] R. Bianco and R. Resta, Mapping topological order in coordinate space, *Phys. Rev. B* **84**, 241106 (2011).
- [39] Q. Marsal, D. Varjas, and A. G. Grushin, Topological Weaire–Thorpe models of amorphous matter, *Proc. Natl. Acad. Sci. U.S.A.* **117**, 30260 (2020).
- [40] J. P. Provost and G. Vallee, Riemannian structure on manifolds of quantum states, *Commun. Math. Phys.* **76**, 289 (1980).
- [41] T. Ozawa and B. Mera, Relations between topology and the quantum metric for Chern insulators, *Phys. Rev. B* **104**, 045103 (2021).
- [42] D. J. Thouless, M. Kohmoto, M. P. Nightingale, and M. Den Nijs, Quantized Hall Conductance in a Two-Dimensional Periodic Potential, *Phys. Rev. Lett.* **49**, 405 (1982).
- [43] C. L. Kane and E. J. Mele, Z_2 Topological Order and the Quantum Spin Hall Effect, *Phys. Rev. Lett.* **95**, 146802 (2005).
- [44] I. Souza, T. Wilkens, and R. M. Martin, Polarization and localization in insulators: Generating function approach, *Phys. Rev. B* **62**, 1666 (2000).
- [45] A. Weiße, G. Wellein, A. Alvermann, and H. Fehske, The kernel polynomial method, *Rev. Mod. Phys.* **78**, 275 (2006).
- [46] See Supplemental Material at [URL will be inserted by publisher] for a detailed description of the polynomial expansion of the quantum geometric tensor, its convergence with the number of moments and size, the density of states in the presence of vacancies and the real space projection of the integrated quantum metric for different phases, energies and concentrations.
- [47] C.-Z. Chang, C.-X. Liu, and A. H. MacDonald, Colloquium: Quantum anomalous hall effect, *Rev. Mod. Phys.* **95**, 011002 (2023).
- [48] H. Chi and J. S. Moodera, Progress and prospects in the quantum anomalous Hall effect, *APL Mater.* **10**, 090903 (2022).
- [49] B. Kramer and A. MacKinnon, Localization: theory and experiment, *Rep. Prog. Phys.* **56**, 1469 (1993).
- [50] A. Cresti, F. Ortmann, T. Louvet, D. Van Tuan, and S. Roche, Broken symmetries, zero-energy modes, and quantum transport in disordered graphene: From supermetallic to insulating regimes, *Phys. Rev. Lett.* **110**, 196601 (2013).
- [51] A. Ferreira and E. R. Mucciolo, Critical delocalization of chiral zero energy modes in graphene, *Phys. Rev. Lett.* **115**, 106601 (2015).
- [52] E. V. Castro, M. P. López-Sancho, and M. A. H. Vozmediano, Anderson localization and topological transition in Chern insulators, *Phys. Rev. B* **92**, 085410 (2015).
- [53] W.-Y. Shan, J. Lu, H.-Z. Lu, and S.-Q. Shen, Vacancy-induced bound states in topological insulators, *Phys. Rev. B* **84**, 035307 (2011).
- [54] S. Roche, N. Leconte, F. Ortmann, A. Lherbier, D. Soriano, and J.-C. Charlier, Quantum transport in disordered graphene: A theoretical perspective, *Solid State Commun.* **152**, 1404 (2012).
- [55] N. Leconte, D. Soriano, S. Roche, P. Ordejon, J.-C. Charlier, and J. J. Palacios, Magnetism-dependent transport phenomena in hydrogenated graphene: From spin-splitting to localization effects, *ACS Nano* **5**, 3987 (2011).
- [56] D. Soriano, N. Leconte, P. Ordejón, J.-C. Charlier, J.-J. Palacios, and S. Roche, Magnetoresistance and magnetic ordering fingerprints in hydrogenated graphene, *Phys. Rev. Lett.* **107**, 016602 (2011).
- [57] J. A. Lawlor, S. R. Power, and M. S. Ferreira, Friedel oscillations in graphene: Sublattice asymmetry in doping, *Phys. Rev. B* **88**, 205416 (2013).
- [58] D. Van Tuan and S. Roche, Spin Manipulation in Graphene by Chemically Induced Pseudospin Polarization, *Phys. Rev. Lett.* **116**, 106601 (2016).
- [59] G. E. Simion and G. F. Giuliani, Friedel oscillations in a Fermi liquid, *Phys. Rev. B* **72**, 045127 (2005).